# Paradoxical Activation of GCN2 by ATP-competitive inhibitors via allosteric activation and autophosphorylation

Graham Neill[1], Vanesa Vinciauskaite[1], Marilyn Paul[2], Rebecca Gilley[3], Simon J. Cook[3], Glenn R. Masson[1*]

1 Division of Cellular and Systems Medicine, School of Medicine, University of Dundee, Dundee, UK
2 Drug Discovery Unit, Wellcome Centre for Anti-Infectives Research, Division of Biological Chemistry, University of Dundee, Dundee DD1 5EH, United Kingdom
3 Signalling Programme, The Babraham Institute, Babraham Research Campus, Cambridge CB22 3AT, U.K.

*Corresponding author: gmasson001@dundee.ac.uk

**Abstract**

Recently it has been found that General Control Non-derepressible 2 (GCN2) can be activated by an array of small molecule ATP-competitive inhibitors, including clinically relevant compounds such as Ponatinib, and compounds specifically designed to be GCN2 inhibitors, such as GCN2iB. Furthermore, we recently showed that GCN2 can be activated in cells by clinically approved small molecule RAF inhibitors. GCN2 is a drug target, specifically in cancers such as mesothelioma, and a better understanding of this paradoxical activation is required to develop drugs which truly inhibit the enzyme. Using biochemical assays and structural mass spectrometry, we present a model for how GCN2 is activated by these compounds by promoting an active conformation in the HisRS domain while competitively inhibiting the kinase domain. This conformation promotes activating phosphorylation of GCN2, potentially through phosphorylation of other activated GCN2 molecules which are not bound to compound. Together this model suggests that efforts to inhibit GCN2 would benefit from exploring allosteric routes rather than targeting the ATP-binding pocket of the kinase domain.

## Introduction

The Integrated Stress Response (ISR) is a crucial stress sensing pathway which protects cells from both external and internal sources of stress. Central to this pathway is the phosphorylation of the α subunit of the eukaryotic initiation factor 2 (eIF2), which results in a global depression in protein synthesis while facilitating the selective transcription of metabolism reprogramming genes which attempt to restore homeostasis [1,2]. In higher eukaryotes, there are four obligate homodimeric eIF2α kinases (GCN2, PKR, PERK, and HRI), all of which sense a unique subset of stresses, become activated, autophosphorylate and subsequently phosphorylate eIF2α on serine 51, triggering the ISR. Given the pivotal role that these kinases have in sensing stress, it is unsurprising that their activity has been found to play a role in several diseases, not least cancer [3–8], which in turn has led to efforts to generate small molecule inhibitors targeting these kinases [9–12].

Activation of GCN2 is complex, requires domain reorganisation, and can occur through multiple diverse routes [13,14]. The current prevailing model is that GCN2 can be activated by amino acid deprivation through either the increased rate of ribosomal collisions or the increased concentration of deacylated tRNA. The ribosomal collision route is thought to be dependent on formation of a complex of the ribosomal collision sensing protein GCN1 [15–17], the ribosomal P-Stalk [18–21], and the kinase Zak-alpha [22], while the tRNA-binding route is simpler, with GCN2 binding directly to deacylated tRNA[13] – recent elegant work by Misra *et al.* has shown that both these routes of activation co-exist and allow GCN2 to respond to different stress sources.

Several recent studies have shown that within a cellular context ATP-competitive inhibitors, even those designed specially to inhibit GCN2, can paradoxically activate GCN2 and the ISR [23–25]. Furthermore, several clinically relevant drugs have also been shown to activate GCN2 *in vivo* [26,27], raising clinically relevant questions on drug mechanisms. Typically, these compounds are inhibitory at high concentrations (> 1 μM), but at lower, approximately nanomolar concentrations, they facilitate GCN2 activation. Previously, a mechanism of how these drugs may facilitate activation was proposed whereby occupancy of compound in the kinase domain in only one of the monomers of GCN2 caused an allosteric activation of the neighbouring monomer [25].

We recently demonstrated that eight BRAF inhibitors, including all clinically approved drugs used in the treatment of melanoma (Dabrafenib, Encorafenib, Vemurafenib) also exhibit paradoxical activation/inhibition of GCN2 [REF Gilley et al.]. In this study we use purified recombinant human GCN2 and found that there was a disconnect between substrate (i.e., eIF2α) phosphorylation and auto-phosphorylation of GCN2, something that is not predicted in current models of GCN2 activation. To further investigate this, we used Hydrogen Deuterium Exchange Mass Spectrometry (HDX-MS) to determine that these compounds, alongside GCN2iB, bind as expected within the active site of the kinase domain of GCN2, but also induce a series of allosteric rearrangements of GCN2, which may account for its activation. Finally, by using a kinase dead mutant of GCN2 (K619R) we show that dimers of GCN2 are capable of phosphorylating other dimers of GCN2 in *trans*, and this is promoted by compound binding. Overall, this presents a new model of how these compounds may facilitate activation of GCN2, which accounts for the low concentration dependency and disconnect between autophosphorylation and substrate phosphorylation.

## Results

*Activation of GCN2 by Kinase Inhibitors produces a characteristic disconnect between kinase autophosphorylation and eIF2α phosphorylation.*

Recently, it has been shown that GCN2 may be activated via ATP-competitive small molecules such as GCN2iB – however, these data derive from cellular experiments, or *in vitro* experiments using fragments of GCN2 [23–25]. For these studies, we used three RAFi that activate GCN2 and the ISR in cells (Dabrafenib, Encorafenib and LY-3009120) and one that fails (GDC-0879) and made comparisons to GCN2iB in a recombinant purified assay using both full length GCN2 enzyme and full length eIF2α substrate. Dabrafenib, Encorafenib, LY-3009120 and GCN2iB activated GCN2 (observed as an increase in the autophosphorylation at p-T899) at low concentrations whereas at high concentrations we observed inhibition (Fig 1A & 1B). In contrast, GDC-0879 had no effect on GCN2 activation. Furthermore, there was an apparent disconnect between the increased levels of GCN2 autophosphorylation (as measured by phosphorylation of T899) and subsequent substrate phosphorylation on eIF2α (as measured by phosphorylation of S51). This disconnect between p-GCN2 and p-eIF2α was not observed when GCN2 was activated by a higher (5x) ATP concentration which caused an increase in both p-eIF2α and p-GCN2 levels.

*Activation of GCN2 occurs at concentrations significantly below binding constants*

The bell-shaped activation curves for GCN2 by RAFi and GCN2iB may suggest multiple binding sites, or different modes of binding. To investigate compound binding, we made use of Thermal Unfolding analysis and Surface Plasmon Resonance (SPR) (see Figure 1A-D, Supplementary Figure 1). Using SPR we found that Dabrafenib, Encorafenib, and LY3009120 all had binding constants of approximately ~50 μM, which is consistent with the $IC_{50}$ values observed on the “down-slope” of the activity assays. Further binding analysis using thermal unfolding, analysis of GCN2 demonstrated a wide range of compound stabilisation effects ranging from +0.6 ºC (LY3009120) to +5.9 ºC for GCN2iB. As per our activity assays, we did not observe binding for GDC-0879 in either binding assay.

*Dabrafenib, Encorafenib, and GCN2iB binding causes allosteric activation of GCN2.* To assess the potential structural changes that accompany compound binding, we conducted Hydrogen Deuterium Exchange Mass Spectrometry (HDX-MS) on full-length human GCN2 in the presence of GCN2iB (see table 1), Dabrafenib and Encorafenib, and as a negative control, GDC-0879. To provide a better three-dimensional context for these HDX-MS data, we created an AlphaFold/ColabFold [28,29] model of human dimeric GCN2 which fulfilled many of the known intramolecular interactions which have been observed previously [30–32], including the recently published structure of the human HisRS-like domain of GCN2[33] (Figure 2B). Mapping HDX-MS data onto this structure we found a good degree of agreement against likely folded sections, loops and areas of disorder (Figure 2C).

Using HDX-MS, we found that Dabrafenib, Encorafenib and GCN2iB all produced distinct changes in solvent exchange, and that GDC-0879 caused no significant changes in exchange rates (See Figures 3 and 4). Dabrafenib, Encorafenib and GCN2iB all bound within the kinase of domain of GCN2, causing large reductions in solvent exchange in peptides surrounding the ATP-binding pocket (residues 587-592, 803-818, 836-876, 902-914) (see Fig 3A, B, C and Fig 4). Surprisingly, compound binding was accompanied by several additional exposures within the kinase domain (861-871, the αC helix (Fig 3C)). Distal from the kinase domain, there are further exposures in GCN2 Unique N-terminal Subdomain of the HisRS (1010-1056) (Figure 3E), the HisRS Domain (1369-1390) (Figure 3E), and the CTD (1591-1633) (see Fig 3D). Comparing the patterns of changed solvent exchange for each of the compounds, Dabrafenib and Encorafenib were most similar in their patterns in exchange, with GCN2iB recreating many of these features also.

*GCN2 can engage in “para-autophosphorylation”*. Current models of GCN2 activation assume that GCN2 can only engage in “cis-autophosphorylation” whereby a GCN2 kinase

domain can phosphorylate its 'own' Thr899 residue (i.e. autophosphorylation within the same polypeptide) or perhaps (with sufficient domain rearrangement) "trans-autophosphorylation" with the Thr899 residue of the dimer partner. We wished to explore whether an activated GCN2 dimer was capable of phosphorylating inactive GCN2 dimers, as this would provide an alternative explanation for how inhibitor-bound GCN2 dimers were capable of becoming phosphorylated. First, we recombinantly expressed and purified a kinase dead mutant of GCN2 – GCN2$^{K619R}$ (See Supplementary Figure 2) [34]. We found the mutant to be a stable dimer (see Supplementary Figure 2), with a melting temperature and profile very similar to that of wtGCN2 (wt GCN2 47.4 ±0.1 ºC, GCN2$^{K619R}$ 47.3 ±0.1 ºC (see Supplementary Fig 2C)) and no detectable autophosphorylation (even after 2 h incubation) or substrate (full length eIF2α) activity, and negligible ATPase activity (See Figure 5A, 5B). Next, to see whether wtGCN2 could phosphorylate GCN2K619R, we immobilised N-terminally strep-tagged wtGCN2 on beads and then incubated the immobilised wtGCN2 with an excess of GCN2 K619R and ATP. Surprisingly, we were able to detect pT899 on catalytically inactivated GCN2 K619R. Furthermore, when we conducted a concentration gradient of Encorafenib in this system, we were able to observe a similar concentration dependent increase in pT899 on GCN2 K619R (See Figure 5D, 5E).

198 **Discussion**
199
200 In this manuscript we use biochemical and structural data to present a model of GCN2
201 activation by small molecule ATP-competitive inhibitors of RAF and GCN2iB. Our recent
202 studies in collaboration with Gilley *et al.* () show that small molecule BRAF inhibitors were
203 effective GCN2 activators in cells, and this was confirmed using our *in vitro* kinase assay.
204 Here we illustrate how these compounds may facilitate GCN2 activation via a mechanism of
205 allosteric activation which is propagated through the enzyme.
206
207 We found that there was a disconnect between the concentration of compound where a
208 peak of GCN2 autophosphorylation was observed and eIF2α phosphorylation could be
209 found. This observation appeared inconsistent with the previous models proposed, where
210 compound occupancy of a single GCN2 monomer facilitated activation of the other monomer
211 within a single GCN2 dimer, thus allowing GCN2 to phosphorylate its substrate i.e., trans-
212 activation, as has been proposed for BRAF/MAPK pathway kinases [35,36]. If this previously
213 suggested model were correct, there should be a typical initial activation
214 autophosphorylation event followed by multiple substrate phosphorylation reactions, as the
215 compound would be acting as an allosteric activator, producing 1:1 correlated p-eIF2α/p-
216 GCN2 levels– however this was not observed. Furthermore, it required a complex array of
217 allosteric interactions that facilitated occupancy of only a single kinase domain, whilst
218 allowing the second kinase domain to remain free of compound. This disagreed with many
219 studies which detailed that GCN2 requires multiple intramolecular rearrangements to
220 achieve autophosphorylation [32,33,37,38], and that there is a reorientation of the kinase domains
221 from an inactive antiparallel to active parallel orientation during activation[39]. One explanation
222 for this discrepancy may be that experiments exploring paradoxical activation of GCN2iB
223 were conducted with isolated fragments of GCN2 where the complex networks of
224 intramolecular allostery that govern GCN2 activation by *e.g.,* tRNA, would presumably be
225 absent [23,24]. Given this apparent discrepancy, we investigated how compounds activate
226 GCN2 using structural mass spectrometry.
227
228 Using HDX-MS, we were able to observe where these compounds were binding to full-length
229 human GCN2 and determine what wider allosteric effects may result from their binding.
230 HDX-MS has been used in several studies to determine the mode of interaction of kinase
231 inhibitors [40–43], and previous investigations using HDX-MS and GCN2 had revealed some of
232 the likely structural changes which occur in GCN2 upon activation via P-stalk binding [18]. We
233 saw a similar pattern of structural changes upon compound binding of Encorafenib,
234 Dabrafenib and GCN2iB with a high degree of solvent exchange reduction within the kinase
235 domain, indicative of compound binding.
236
237 To note, GCN2 has three potential ATP-binding sites: namely, the canonical kinase domain,
238 and the more cryptic sites in the pseudokinase and HisRS domains. We only observed
239 reductions in solvent exchange (indicative of a direct interaction) in the kinase domain site;
240 this is consistent with our previous modelling predictions and expression of gatekeeper
241 mutations in cells (Gilley et al.) However, there were also several unexpected increases in
242 solvent exchange distal to the ATP-binding site of the kinase domain, and thus these
243 increases in HDX are likely to be the result of the breaking of auto-inhibitory hydrogen
244 bonding networks – similar events have been observed before with other allosteric activation
245 events [44].
246
247 Previous mutagenesis studies of GCN2/Gcn2 have provided insight into the network of
248 interactions which facilitate autoinhibition and subsequent activation of the enzyme [30,38,45,46].
249 These hydrophobic residues and autoinhibitory interactions span the enzyme but form a
250 nexus on L869 (L856 in yeast Gcn2) – a residue that follows directly after the 'DFG' of the
251 activation loop of the kinase domain, and strands β3 or β5 and the helix αC [30]. Our HDX data
252 shows all the activating compounds influencing these elements of the kinase domain, and

253 thus it may be triggering this network of interactions. Most apparent for its disruption of the
254 αC helix was Dabrafenib, binding of which resulted in an increase in solvent exchange in this
255 area. Dabrafenib binding may disrupt the hydrophobic node formed by I633, V637 and L639,
256 and may also influence by the breaking of the inactivating salt bridge which forms between
257 E636 (also in the αC and R847 (in the catalytic loop)[46] – all these regions saw changes in
258 the solvent exchange upon Dabrafenib, Encorafenib and GCN2iB binding.
259
260 Other regions crucial for GCN2 activation are the C-terminal domain (CTD) and the histidyl-
261 tRNA synthetase (HisRS) domains - the interplay between these two domains has been
262 demonstrated to be key for GCN2 activity [37]. Within the HisRS domain we saw increases in
263 solvent exchange in residues 1369-1390 (Fig 3E) – this region was found be the most
264 protected in a recent publication mapping tRNA biding to the isolated HisRS domain [33] –
265 thus the H-bonds network appears to be melting the structure in this region typically
266 associated with tRNA interaction. This may be indicative of a "priming" of the site for tRNA
267 binding. Mutagenesis of D1353 (yeast D1327) to either alanine or lysine completely
268 abrogates GCN2 activity [37] –the recently published human HisRS domain structure [33] shows
269 D1353 near to the region of exposure produced upon RAFi/GCN2iB binding, which may
270 suggest that this region acts a gatekeeper for activation of the enzyme.
271
272 In our AlphaFold/ColabFold model of GCN2, the N-terminus of the HisRS domain sits in very
273 close proximity to both the PKD and KD domains – this may provide insight into how binding
274 within the kinase domain is propagated through the HisRS domain. The HDX-MS data
275 shows that there are increases in solvent exchange on compound binding in a helical bundle
276 found within the first 50 residues of the HisRS domain (1010-1055), and proximate to this
277 bundle is a cradle of beta-hairpin loops of the PKD β3/β4 strands (residues 299-309). The
278 helical bundle – referred to as the "GCN2 Unique N-terminal Subdomain" by Yin *et al.* [33], sits
279 directly above the ATP binding loop of the HisRS domain -and in our model, may facilitate
280 the propagation of allostery. Given these compounds appear to be "priming" GCN2 for
281 activation by either the CTD or HisRS domains, investigating whether these routes to
282 activation are promoted by compound binding requires further investigation.
283
284 Dabrafenib, Encorafenib and GCN2iB binding in the kinase domain caused structural
285 changes in the CTD, even though it is approximately 80 Å away from the binding site with
286 our model. This increase in HDX suggests a breakdown of the hydrogen bonding in this
287 region – although interpreting this change in solvent exchange is difficult. Mapping the
288 peptides covering the region of the (1591-1637) to the murine and yeast crystal structures
289 produced of the CTD dimer (Supplementary Figure 3) [47], we see that the exposure is largely
290 confined to a pair of helices that present away from the dimeric interface. A key residue for
291 maintaining the CTD dimer, L1587, is nearby, but does not show increased exposure on
292 compound binding. Truncation analysis in yeast found that part of the CTD could directly
293 bind to the ribosome [48] – although the construct used did not contain the 1591-1637 helix –
294 its exact function is currently unknown. Overall, our HDX-MS data supports a model of
295 catalytic inhibition coinciding with a partially activated structure where many known points of
296 regulation have become more flexible.
297
298 The 'activation' of GCN2 has frequently been synonymous with both autophosphorylation of
299 T899 and eIF2α phosphorylation - however, our analysis has shown that phosphorylation
300 can effectively be de-coupled from eIF2α by these ATP-competitive compounds.
301 Furthermore, "true" activation of GCN2 by tRNA or ribosomal binding has often been
302 associated with large rearrangements of GCN2, especially with the kinase domain adopting
303 an inactive antiparallel stance which then rearranges to an active parallel dimer via
304 activation[39]. Our HDX-MS data show that these compounds activate GCN2 but do not
305 appear to induce the large-scale rearrangements that would be necessary to facilitate a shift
306 from antiparallel to parallel arrangement of the kinase domain – strengthening the possibility

that these compounds are essentially catalytically inhibiting, while facilitating phosphorylation of GCN2.

Finally, we observed that GCN2 may be capable of phosphorylating in *trans* – and that the ATP-competitive compounds can make GCN2 a better substrate for *trans* phosphorylation by presenting a pseudo-active state. However, further research will be required to determine whether this sequence of events is what occurs in a cellular context. It raises the possibility that there is the potential for a positive feedback loop occurring whereby activation of minor populations of GCN2 allows for a burst of activating trans phosphorylation events and the rapid amplification of the ISR – something which may be required if the initiating event – frustrated ribosomal collision[1522], is a relatively low-frequency/density occurrence in the cell.

The observation that a wide array of ATP-mimetic kinase inhibitors, including those that are clinically approved and are thought to act through alternate signalling pathways can activate GCN2 within a cellular context has implications for drug discovery, not least in the efforts to target GCN2. This is especially noteworthy in cancer cells where, in response to the compounds, there will be a selective pressure to alter GCN2 concentrations to facilitate cell growth[49,50]. If it is beneficial within certain pathologies to inhibit GCN2, it may be worthwhile employing a drug discovery programme that avoids ATP-competitive compounds and instead attempts to inhibit GCN2 by allosteric means, or targeted protein degradation (i.e., proteolysis targeting chimeras (PROTACs)).

329 **Figure Legends:**
330
331 **Figure 1: RAFi and GCN2iB promote GCN2 autophosphorylation, but not eIF2α**
332 **phosphorylation. (A)** Activity assay of human recombinant GCN2 phosphorylating eIF2α
333 against a concentration gradient of LY3009120. **(B)** Quantified assays against 5 compounds
334 – LY3009120, Dabrafenib, Encorafenib, GDC0879 and GCN2iB. pThr899 GCN2 levels peak
335 at ~1 μM for Dabrafenib, Encorafenib and GDC0879, and 10 nM for GCN2iB. GDC0879
336 does not appear to alter GCN2 activity **(C)** pS51 EIF2α levels across a gradient of
337 compounds. **(D)** Thermal Unfolding assays of GCN2 against compounds. Lines represent
338 nadirs of the first inflection point.
339
340 **Figure 2: Predicted Model of GCN2 generated by AlphaFold/Collabfold and**
341 **comparison to HDX-MS data. (A)** Domain organisation and amino acid residue boundaries
342 for human GCN2. CL = Charged Linker, PKD = pseudokinase domain, HisRS = Histidyl
343 synthetase like domain, CTD = C-terminal Domain **(B)** Views of the GCN2 dimer generated
344 using AlphaFold/Colabfold. CLH = charged linker helix, KIL = kinase insertion loop. **(C)** HDX-
345 MS data for APO GCN2. Typically, regions where deuterium uptake is greater than 50%
346 (shown as the dashed line) at 0.3s incorporation are likely unstructured loops with his
347 flexibility.
348
349 **Figure 3: HDX-MS changes associated with Dabrafenib binding. (A)** Selected peptides
350 showing the effect of Dabrafenib binding to GCN2. * = Greater than 5% & 0.5Da change,
351 passes t-test at p=0.05. Error bars may be smaller than the points on the graph. **(B)**
352 Dabrafenib binding mapped onto the entire GCN2 model. Cooler colours represent areas of
353 'protection' (i.e., slower solvent exchange rate), warmer colours show 'exposure' (i.e.,
354 increased solvent exchange rate). **(C)** Inset of the kinase domain of GCN2 showing HDX
355 changes on Dabrafenib binding. T899, a "bell weather" site of autophosphorylation and
356 activation is highlighted. **(D)** The C-Terminal Domain of GCN2, highlighting the exposure of
357 the helical hairpin found in residues 1591-1633. **(E)** The His-RS Like Domain with the GCN2
358 Unique N-terminal Subdomain included, highlight the exposure occurring in this domain.
359 Dashed lines represent 2-fold symmetry of the dimer.
360
361 **Figure 4: Comparison of HDX-MS changes with (A) Dabrafenib (B) Encorafenib (C)**
362 **GCN2iB (D) GDC0876.** Each point in the midpoint of a peptide with the five-points in
363 gradually more saturated colours. Black points/line are the SUM difference across all
364 timepoints. **(E)** Amalgamated changes mapped onto one another. Inset is a principal
365 component analysis comparing all the data summed data.
366
367 **Figure 5: GCN2 is capable of phosphorylating in *trans* (A)** Autophosphorylation activity
368 comparison of wtGCN2 with $GCN2^{K619R}$. **(B)** Comparison of ATPase activity as measured
369 using ADPGLO between GCN2 and $GCN2^{K619R}$. **(C)** Thermal Unfolding Assay for $GCN2^{K619R}$
370 on compound binding. **(D)** Western Blot analysis of trans-phosphorylation of GCN2. **(E)**
371 Compound-driven trans phosphorylation of $GCN2^{K619R}$ by immobilised wtGCN2 by
372 Encorafenib.
373
374 **Supplementary Figure 1: Binding of Compounds to GCN2 (A)** SPR traces of binder
375 Dabrafenib and non-binder GDC-0879 **(B)** Steady-State analysis of compound binding
376 derived from SPR **(C)** Amalgamated compound characteristics. *Both Encorafenib and
377 GCN2iB demonstrated binding with SPR, producing a concentration dependent response,
378 but at the analytes at higher concentrations shows superstoichiometry. Combined with the
379 fast kinetic on and off rates, affinities determined are less accurate.
380
381 **Supplementary Figure 2: Characterisation of $GCN2^{K619R}$ (A)** Gel Filtration profile of
382 wtGCN2 (red) and $GCN2^{K619R}$ (green) showing similar elution profiles **(B)** SDS-PAGE of Gel

383 Filtration of fractions of GCN2$^{K619R}$ **(C)** Thermal denaturation profile of wtGCN2 (red) and
384 GCN2$^{K619R}$ (green).
385
386 **Supplementary Figure 3: Comparison of CTDs.** The CTDs of Human (produced by
387 Alphafold), Mouse (crystal structure PDB: 4OTN), and Yeast (4OTM), with the helix-turn-
388 helix motif which exhibited an increase in HDX-MS on compound binding shown in orange.
389
390
391 **Table 1.0 HDX-MS Statistics**
392

| | Apo | GDC | Dab | Enc | GCN2iB |
|---|---|---|---|---|---|
| **# of Peptides** | 687 | | | | |
| **Coverage** | 95.4% | | | | |
| **Av. Length** | 13.2 a.a. | | | | |
| **Redundancy** | 5.5 | | | | |
| **Time Points** | 0.3s*/3s/30s/300s/3000s | | | | |
| **Replicates** | 3 per time point. 5 ND. | | | | |
| **Controls** | Non-Deuterated and Maximally Deuterated Control | | | | |
| **Replicability** | Average % STDEV for technical triplicate = 1.00% | | | | |
| **Significance threshold** | >5σ & t test <0.05 | | | | |

393
394 ***** 0.3s timepoint created by conducting a 3 s timepoint on ice.
395
396 **Acknowledgements**
397 GRM and GN are supported by a Baxter Fellowship from the University of Dundee, and a
398 TENOVUS grant T21/01 119615, and Biotechnology and Biological Sciences Research
399 Council (UKRI-BBSRC) Capital Equipment Grant BB/V019635/1. VV supported by MRC
400 iCase Studentship (MR/R01579/1). R.G. and S.C. were Plexxikon Inc and Institute Strategic
401 Programme Grants BB/J004456/1, BB/P013384/1 and BB/Y006925/1 from the UKRI-
402 BBSRC.
403
404 **Competing Interests Statement**
405 The authors announce no competing interests. The initial stages of this work (i.e.
406 identification of RAFi/GCN2 activation in a cellular context) were supported by sponsored
407 research collaboration in SJC's laboratory funded by Plexxikon Inc.
408
409 **Materials and Methods**
410
411 *Antibodies and Reagents*
412 Primary Anitbodies: Total EIF2S1 (eIF2α) (1:1000 WB, SC133132, Santa Cruz),
413 phosphoserine 51 EIF2S1 (1:500 WB, 9721S, Cell Signalling Technology), Total GCN2
414 (1:1000 WB, MA5-32704, Invtirogen), phosphothreonine 899 GCN2 (1:1000 WB, AB75836
415 , Abcam) 6X His Tag (1:1000 WB, R931-25, Invitrogen),
416
417 Secondary Antibodies: IRDye® 680RD Goat anti-Mouse IgG Secondary Antibody (926-
418 68070, Licor), IRDye® 800CW Goat anti-Mouse IgG Secondary Antibody (926-32210,
419 Licor), IRDye® 800CW Donkey anti-Rabbit IgG Secondary Antibody (926-32213
420 , Licor), IRDye® 680RD Goat anti-Rabbit IgG Secondary Antibody (926-68071
421 , Licor).
422
423 *GCN2 Expression and Purification*
424 Expression and purification of recombinant human GCN2 was conducted as described
425 previously[18]. Briefly, human GCN2 cloned (uniprot ID: Q9P2K8) was cloned into a
426 baculoviral vector with an N-terminal twin StrepII tag followed by a TEV protease site.

427 Plasmids were then integrated into the EMBacY baculoviral DNA, and the baculovirus
428 amplified over three rounds. GCN2 was then expressed in *Sf9* cells by infecting cells at a
429 density of 1.5x $10^6$ cells/mL with 15 mL of virus being used per 500 mL of cells. Cells were
430 grown at 27 ºC for 55 hours and were then harvested via centrifugation, washed in ice cold
431 PBS and snap frozen in liquid nitrogen. Pellets were then thawed on ice with 100 mL of Lysis
432 Buffer A (20 mM Tris pH 8.0, 150 mM NaCl, 5% v/v glycerol, 2 mM β-mercaptoethanol
433 (BME), and one cOmplete EDTA-free protease inhibitor tablet per 50 mL of Buffer). Cells
434 were then lysed via probe sonication, on ice, for 5 min (10 s on/ 10 s off), and then
435 Benzonase at 2 U/mL was added. Lysate was then centrifuged at 140,000 *g* at 4 ºC for 45
436 minutes. Proteins were purified using an AKTA protein purification system (Cytiva). The
437 supernatant was then filtered through a 0.2 µm syringe filter before being loaded onto 2 x 5
438 mL StrepTrap HP Columns (GE Healthcare Life Sciences 28-9075-47), equilibrated in Step
439 A Buffer (20 mM Tris pH 8.0, 150 mM NaCl, 5% v/v glycerol, 2 mM BME) at a flow rate of 4
440 mL/min. Protein was then eluted through a gradient of Strep B Buffer (20 mM Tris pH 8.0,
441 150 mM NaCl, 5% v/v glycerol, 2 mM BME, 6 mM desthiobiotin). Peak fractions were
442 analysed using SDS-PAGE and assessed for relative purity. GCN2-containing fractions were
443 then diluted using $Q_0$ Buffer (20 mM Tris pH 8.0, 5% v/v glycerol) to a NaCl concentration of
444 ~50 mM before being loaded onto a 5 mL HiTrap Q HP column (Cytiva 17115401),
445 equilibrated in QA Buffer (20 mM Tris pH 8.0, 50 mM NaCl, 5 & v/v glycerol, 2 mM BME), at
446 a flow rate of 4 mL/min. The column was then washed with 100 mL QA Buffer, before a
447 gradient of QB Buffer (20 mM Tris pH 8.0, 1 M NaCl, 5% v/v glycerol, 2 mM BME) was
448 applied. GCN2 containing fractions were then pooled and concentrated using a 50 mL
449 Amicon Centrifugation Concentrator (50k MWCO) to a volume of ~1 mL before being
450 injected onto a Hi Load 16/60 Superdex 200 column (Cytiva/GE Healthcare 28989335),
451 equilibrated with GF buffer (20 mM HEPES pH 7.5, 150 mM NaCl, 2 mM tris(2-
452 carboxyethyl)phosphine (TCEP)), at a flow rate of 1 mL/min. GCN2 containing fractions were
453 concentrated using a 50 mL concentrator to a concentration of ~3 mg/ml before being
454 aliquoted and snap frozen in liquid nitrogen.
455
456 *$GCN2^{K619R}$ Expression and Purification:*
457 Human wtGCN2 was mutated via QuickChange mutagenesis to K619R (Forward Primer:
458 GGACGGTTGCTGCTACGCTGTGAGGCGTATCCCCATCAACCCTGC, reverse:
459 CGGGAAGCAGGGTTGATGGGGATACGCCTCACAGCGTAGCAGC). Expression and
460 purification proceeded as per wtGCN2, except after the Strep-Tag-purification, GCN2 K619R
461 was cleaved for 16h at 4ºC with TEV protease to remove an N-terminal His-Strep Tag.
462 Purification then proceeded as per wtGCN2 (Q Column and Gel Filtration in the same
463 buffers). Fractions were concentrated to 5.5 mg/mL and stored as per wtGCN2.
464
465 *eIF2α Expression and Purification:* Expression and purification of recombinant human eIF2α
466 was conducted as described previously[18]. DNA encoding full-length human eIF2α (NCBI
467 reference number: NP_004085.1) was inserted into the vector pOPTH with an N-terminal
468 His6 tag followed by a TEV protease site. The plasmid was transformed into chemically
469 competent BL21 Star (DE3) cells, and cells were grown overnight before being inoculated to
470 a 50 mL starter culture in 2xTY media containing 0.1 mg/mL Ampicillin. The starter culture
471 was incubated at 37 ˚C for 90 minutes, then 10 mL starter culture was added to 4 x 900 mL
472 2xTY media containing Ampicillin. Cultures were incubated at 37 ˚C until the optical density
473 reached 0.7, and then protein expression was induced by the addition of 0.3 mM isopropyl β-
474 D-1- thiogalactopyranoside (IPTG). Cells were grown for a further 3 hours at 37 ˚C before
475 being harvested, washed with ice-cold phosphate-buffered saline and frozen in liquid
476 nitrogen. Bacterial cell pellets were lysed in 100 mL Lysis Buffer (20 mM Tris-HCl pH 8.0,
477 100 mM NaCl, 5 % v/v glycerol, 2 mM BME 0.5 mg/mL Lysozyme (Sigma L6876), 2 U/mL
478 Benzonase, one cOmplete EDTA-free protease inhibitor tablet (Roche 04693132001) per 50
479 mL of Buffer). Cells were lysed using a probe sonicator for 5 minutes (10 s on/ 10 s off) and
480 then centrifuged at 140,000 *g* for 45 min at 4 ˚C. The supernatant was filtered through a 0.2
481 µm syringe filter before being loaded onto a 5 mL HisTrap HP Column (Cytiva 17524801)

482 equilibrated in Ni A Buffer (20 mM Tris pH 8.0, 100 mM NaCl, 5 % v/v glycerol, 10 mM
483 imidazole pH 8.0, 2 mM BME), followed by the elution of protein via a gradient of Ni B Buffer
484 (20 mM Tris pH 8.0, 100 mM NaCl, 5% v/v glycerol, 200 mM Imidazole pH 8.0, 2 mM BME).
485 Protein purification then proceeded as described for GCN2. Proteins were concentrated to
486 ~10 mg/mL and then snap frozen in liquid nitrogen.
487
488 *Thermal Unfolding Assays:* Thermal Unfolding Assays were conducted using a NanoTemper
489 Panta using Prometheus Standard Capillaries (NanoTemper) (PR-C002). Briefly,
490 GCN2/GCN2 K619R was defrosted, and centrifuged at 20,000 *g* for 10 minutes, and then
491 diluted to 0.3 mg/mL in 20 mM HEPES pH 7.5, 150 mM NaCl, 1 mM TCEP Buffer was
492 incubated with compounds on ice for 45 minutes before being analysed. A gradient of 1
493 ºC/min was applied to the sample starting from 25 ºC to 85 ºC. Fluorescence at 330 nm and
494 350 nm was monitored using an excitation wavelength of 280 nm. Data analysis and
495 identification of inflection points/TMs was conducted using the Panta Analysis Software
496 (NanoTemper).
497
498 *Surface Plasmon Resonance (SPR) Studies:* SPR studies were carried out using Biacore T-
499 200 (GE Healthcare) and Biacore 8K+ (Cytiva) using Series S NTA Sensor Chips (Cytiva).
500 The running buffer was HBS-P+ (Cytiva) with 1% DMSO, with the flow cell temperature held
501 at 25 ºC, and the sample compartment temperature held at 10 ºC. His-tagged
502 GCN2/GCN2$^{K619R}$ at a concentration of 0.05 mg/mL was immobilised using custom capture-
503 immobilization method to an RU of ~8600RU. Ligands were captured on pre-conditioned
504 chips activated in 2 steps first by NiCl2 followed by a 1:1 mixture of 1-ethyl-3-(3-
505 dimethylaminopropyl)-carbodiimide hydrochloride (EDC) and N-hydroxysuccinimide (NHS).
506 Analyte binding studies was performed using 12-point dose response curve. Two
507 concentration series starting from 150 µM were prepared for each compound from 10 mM
508 stocks in 100% DMSO. Dilutions of analyte were prepared in 1xHBS-P+ at final
509 concentration of 1%-1.5% DMSO. Analysis step included and association time of 60s and
510 dissociation time of 120 s, at a flow rate of 40 µL/min. Data was collected at a rate of 10 Hz
511 using T200 Control software Version 2.0.1 in High performance mode and analysed using
512 Biacore Insight Evaluation Software™-Version 5.0.18.22102. Solvent correction was
513 performed using 6-point linear concentration range between 0.2%- 1.8% DMSO. Data
514 analysis was performed on the solvent corrected, blanked curves using a 1:1 binding (Rmax
515 constant at Ymax) model and steady state affinity (constant Rmax, 10RU per 100Da) model
516 for a response window of 5 s at 5 s before end of injection (equilibrium analysis) for relevant
517 concentrations. Steady state affinities and kinetic data have been used for qualitative
518 assessment of target binding.
519
520 *GCN2 Activity Assays*
521 *ADP-GLO:* Using a PROMEGA ADP-GLO Kinase assay, 100 nM GCN2 was incubated with
522 50 µM polyarginine-serine repeat peptide (Sigma-Aldrich SRP0683) or 10 µM eIF2α with
523 500 µM ATP in 1 x Kinase Reaction Buffer (20 mM Tris pH 8.5, 0.2 mM EDTA, 0.1 % Tween
524 20, 100 mM NaCl, 0.001% Brij-35, 0.5% glycerol, 10 mM MgCl2, 0.1 mg/mL BSA) for 1 hour
525 at room temperature, until the reaction was quenched using the ADP-GLO Reagent.
526
527 *Phos-tag Gels*: Phos-tag gel assays were also conducted to facilitate relative substrate
528 phosphorylation and autophosphorylation levels. 400 nM GCN2 was incubated with 14 µM
529 eIF2α and 250 µM ATP and 50 µM deacylated tRNA in 20 mM Tris pH 8.0, 150 mM NaCl,
530 10 mM MgCl2 at 30 °C. Reactions were quenched through mixing with 2xSDS-PAGE
531 Loading buffer with 1 mM ZnCl2. 10 µL of reactions were loaded onto SuperSep Phos-tag
532 (50 µmol/L) 100 x 100 x 6.6 mm (17 well) gels (Fujifilm). Gels were run in the manufacturer's
533 suggested 100 mM Tris pH 7.8/ 100 mM MOPS/ 0.1% SDS / 5 mM Sodium Bisulfite solution.
534 Gels were held at a constant 100 V for 2 h prior to staining with InstantBlue Coomassie Stain
535 (AbCam).
536

537 *Western-Blot*: 10 nM GCN2 was incubated at 30 ºC for 20 min with 2 µM eIF2α and 10 µM
538 ATP in varying deacylated tRNA concentrations. Samples were then quenched via the
539 addition of SDS-PAGE loading buffer and heating to 95 ºC for 3 min. Samples were then run
540 in a MES buffer SDS-PAGE experiment using a 15 well 5-12% Bis-Tris Gel, run at 180 V for
541 35 min at RT. Gels were then briefly incubated in 20% ethanol solution prior to a transfer to a
542 nitrocellulose membrane using the iBlot 2 Transfer system. Membranes were then blocked
543 using 5% Milk TBST solution for 1 hour at RT, before being washed three times 10 min
544 incubation with TBST. Primary antibodies were diluted as follows in 4% BSA TBST: total
545 eIF2alpha (Santa Cruz Biotechnology sc-133132) 1:1000, phospho-eIF2S1 Ser51 (Cell
546 Signalling Technology 9721) 1:500, total GCN2 (Invitrogen JA03-83) 1:1000, pThr899 GCN2
547 (Abcam AB75836) 1:1000. Primary antibody solutions were incubated with membranes in
548 heat-sealed bags with gentle agitation for 1 h at RT or overnight at 4 ºC. Membranes were
549 then washed 3 x 10 min with TBST. Secondary antibodies (LICOR IRDye 800 CW (926-
550 32210 and 926-32213) were then prepared to manufacturer's instructions (0.5 µL in 5 mL
551 4% BSA TBST) and incubated for 1 h in a 50 mL Falcon tube on a roller. Membranes were
552 washed with 3 x 10 min TBST before imaging with a LICOR Odyssey FC. Images were
553 captured and quantified in Image Studio Ver 5.2.
554
555 *Immobilised GCN2$^{K619R}$ Activity Assay:* 25 µL (per reaction) of IBA Strep-Tactin Sepharose
556 resin was washed with Reaction Buffer (20 mM Tris pH 7.5, 150 mM NaCl, 50 mM $MgCl_2$, 1
557 mM TCEP) five times via resuspension and centrifugation. 100 µL of 20 nM Strep-Tagged
558 wtGCN2 was immobilized on resin for 1 h at 4 ºC with agitation, followed by five more
559 washes with twice the bead volume. Resin was then incubated with 2 µM non-tagged
560 GCN2$^{K619R}$, 10 µM and compound in a 50 µL final volume (i.e., 50% beads with 20 nM wt-
561 GCN2 bound for a final concentration of 10 nM wt-GCN2). The reaction was incubated for 20
562 min at 30 ºC. The reaction was quenched via separating the beads and substrate GCN2$^{K619R}$
563 via centrifugation using a Cytiva MicroSpin Column, and the flowthrough was then mixed
564 with SDS-PAGE loading buffer and boiled at 94 ºC for 3 minutes. The beads were then
565 further washed twice to remove residual GCN2$^{K619R}$, followed by elution using Elution Buffer
566 (20 mM Tris pH 8.0, 150 mM NaCl, 5 mM desothiobiotin, 1 mM TCEP). GCN2
567 phosphorylation was measured using Western Blots as described above.
568
569 *Hydrogen Deuterium Exchange Mass Spectrometry*
570 *Sample Preparation:* 5 µM GCN2 was incubated with or without 100 µM Compound (as
571 stated) for 30 minutes in Protein Dilution Buffer (20 mM HEPES pH 7.5, 150 mM NaCl, 15
572 mM MgCl2, 2 mM TCEP). 5 µL of this sample was diluted with 45 µL of Deuteration Buffer
573 (20 mM HEPES pH 7.5, 150 mM NaCl, 15 mM MgCl2, 2 mM TCEP, 1% DMSO, 96.5 %
574 D2O) (final D2O concentration = 85.95%) for timepoints 3/ 30/ 300/ 3000 s, before being
575 quenched with 20 µL of ice cold Quench Solution (6 M Urea, 2% Formic Acid), and being
576 snap frozen in liquid nitrogen and stored at – 70 ºC. A further timepoint, 0.3 s, was achieved
577 by incubating both the sample and deuteration buffer on ice and then conducting a 3 s
578 exchange reaction. Each exchange reaction was conducted independently four times.
579
580 *Data Acquisition:* Data acquisition was conducted broadly as previously described[44].
581 Samples were rapidly thawed at room temperature and then injected into automated HDX-
582 MS fluidics and UPLC manager system (Waters). Samples were loaded into a 50 µL loop
583 and then subsequently digested using a Waters Enzymate BEH Pepsin Column (Part No.
584 186007233) in a 0.1 % Formic Acid solution with a flow rate of 200 µL/min at 20 ºC. Peptic
585 peptides then flowed onto a Waters ACQUITY UPLC BEH C18 VanGuard Pre-Column at 1
586 ºC (Part No. 186003975). After digestion, the flowpath was changed to elute the peptides via
587 a Waters ACQUITY UPLC BEH C18 1.7 µm 1.0 x 100 mm reverse phase column (Part No.
588 186002346). A gradient from 0-85% 0.1% Formic Acid/ Acetonitrile, conducted at 1 ºC with a
589 40 µL/min flowrate was used to elute deuterated peptides which were then ionised using an
590 ESI source. Mass spectrometry data were collected using a Waters Select Series cIMS
591 instrument, from a 50-2,000 m/z range with the instrument in HDMSe mode. A single pass of

592 the cyclic ion mobility separator (with a cycle time of 47 ms) was conducted. A blank sample
593 of protein dilution buffer with quench was run between samples, and carryover was routinely
594 checked to be <1% intensity of the prior sample.
595
596 *Data Analysis:* Peptide sequence identification was conducted using Protein Lynx Global
597 Server (Waters). Minimum inclusion criteria were a minimum intensity of 5000 counts,
598 minimum sequence length 5, maximum sequence length 35, a minimum of 3 fragment ions,
599 a minimum of 0.1 products per amino acid, a minimum score of 5.0, a maximum MH+ Error
600 of 10 ppm. Subsequent analysis and determination of deuteration values conducted using
601 HDExaminer (Sierra Analytics/Trajan).
602
603 **CRediT Author Contribution**
604 Graham Neill: Conceptualisation, Investigation, Formal analysis, Writing — review and
605 editing. Vanesa Vinciauskaite: Resources, Investigation, Writing — review and editing.
606 Marilyn Paul: Investigation, Formal Analysis. Rebecca Gilley: Investigation, Writing — review
607 and editing. Simon Cook: Conceptualisation, Resources, Writing – review and editing. Glenn
608 R Masson: Conceptualisation, Resources, Supervision, Investigation, Funding acquisition,
609 Methodology, Writing — original draft, Project administration, Writing — review and editing.
610

611 1. Wek, R. C. Role of eIF2α Kinases in Translational Control and Adaptation to Cellular
612 Stress. *Cold Spring Harbor Perspectives in Biology* **10**, a032870 (2018).

613 2. Zebrucka, K. P. *et al.* The integrated stress response. *EMBO reports* **17**, 1374–1395
614 (2016).

615 3. Schmidt, S. *et al.* A MYC-GCN2-eIF2α negative feedback loop limits protein synthesis to
616 prevent MYC-dependent apoptosis in colorectal cancer. *Nature Cell Biology* **21**, 1413–1424
617 (2019).

618 4. Wang, Y. *et al.* Amino Acid Deprivation Promotes Tumor Angiogenesis through the
619 GCN2/ATF4 Pathway. *Neoplasia* **15**, 989–997 (2013).

620 5. Kardos, G. R., Wastyk, H. C. & Robertson, G. P. Disruption of Proline Synthesis in
621 Melanoma Inhibits Protein Production Mediated by the GCN2 Pathway. *Mol. Cancer Res.*
622 **13**, 1408–1420 (2015).

623 6. Saavedra-García, P. *et al.* Systems level profiling of chemotherapy-induced stress
624 resolution in cancer cells reveals druggable trade-offs. *Proc National Acad Sci* **118**,
625 e2018229118 (2021).

626 7. Parzych, K. *et al.* The coordinated action of VCP/p97 and GCN2 regulates cancer cell
627 metabolism and proteostasis during nutrient limitation. *Oncogene* **38**, 3216–3231 (2019).

628 8. Cordova, R. A. *et al.* GCN2 eIF2 kinase promotes prostate cancer by maintaining amino
629 acid homeostasis. *Elife* **11**, (2022).

630 9. Nakamura, A. *et al.* Inhibition of GCN2 sensitizes ASNS-low cancer cells to asparaginase
631 by disrupting the amino acid response. *P Natl Acad Sci Usa* **115**, E7776–E7785 (2018).

632 10. Lough, L. *et al.* Triazolo[4,5-d]pyrimidines as Validated General Control
633 Nonderepressible 2 (GCN2) Protein Kinase Inhibitors Reduce Growth of Leukemia Cells.
634 *Comput Struct Biotechnology J* **16**, 350–360 (2018).

635 11. Fujimoto, J. *et al.* Identification of Novel, Potent, and Orally Available GCN2 Inhibitors
636 with Type I Half Binding Mode. *Acs Med Chem Lett* **10**, 1498–1503 (2019).

637 12. Kato, Y. *et al.* GZD824 inhibits GCN2 and sensitizes cancer cells to amino acid
638 starvation stress. *Mol Pharmacol* MOLPHARM-AR-2020-000070 (2020)
639 doi:10.1124/molpharm.120.000070.

640 13. Misra, J., Carlson, K. R., Spandau, D. F. & Wek, R. C. Multiple mechanisms activate
641 GCN2 eIF2 kinase in response to diverse stress conditions. *Nucleic Acids Res.* gkae006
642 (2024) doi:10.1093/nar/gkae006.

643 14. Masson, G. R. Towards a model of GCN2 activation. *Biochem Soc T* **47**, 1481–1488
644 (2019).

645 15. Pochopien, A. A. *et al.* Structure of Gcn1 bound to stalled and colliding 80S ribosomes.
646 *Proc National Acad Sci* **118**, e2022756118 (2021).

647 16. Yamazaki, H. *et al.* Ribosome binding protein GCN1 regulates the cell cycle and cell
648 proliferation and is essential for the embryonic development of mice. *Plos Genet* **16**,
649 e1008693 (2020).

650 17. Sattlegger, E. & Hinnebusch, A. G. Polyribosome Binding by GCN1 Is Required for Full
651 Activation of Eukaryotic Translation Initiation Factor 2α Kinase GCN2 during Amino Acid
652 Starvation. *J Biol Chem* **280**, 16514–16521 (2005).

653 18. Inglis, A. J. *et al.* Activation of GCN2 by the ribosomal P-stalk. *Proc National Acad Sci*
654 **116**, 201813352 (2019).

655 19. Gupta, R. & Hinnebusch, A. G. Differential requirements for P stalk components in
656 activating yeast protein kinase Gcn2 by stalled ribosomes during stress. *Proc National Acad*
657 *Sci* **120**, e2300521120 (2023).

658 20. Deryło, K. *et al.* The uL10 protein, a component of the ribosomal P-stalk, is released
659 from the ribosome in nucleolar stress. *Biochimica et Biophysica Acta (BBA) - Molecular Cell*
660 *Research* **1865**, 34–47 (2018).

661 21. Harding, H. P. *et al.* The ribosomal P-stalk couples amino acid starvation to GCN2
662 activation in mammalian cells. *eLife* **8**, 1 (2019).

663 22. Wu, C. C.-C., Peterson, A., Zinshteyn, B., Regot, S. & Green, R. Ribosome Collisions
664 Trigger General Stress Responses to Regulate Cell Fate. *Cell* **182**, 404-416.e14 (2020).

665 23. Carlson, KennethR., Georgiadis, MillieM., Tameire, F., Staschke, KirkA. & Wek,
666 RonaldC. Activation of Gcn2 by small molecules designed to be inhibitors. *J Biol Chem*
667 104595 (2023) doi:10.1016/j.jbc.2023.104595.

668 24. Szaruga, M. *et al.* Activation of the integrated stress response by inhibitors of its kinases.
669 *Nat. Commun.* **14**, 5535 (2023).

670 25. Tang, C. P. *et al.* GCN2 kinase activation by ATP-competitive kinase inhibitors. *Nat*
671 *Chem Biol* **18**, 207–215 (2022).

672 26. Ciudad, M. T. *et al.* Dabrafenib alters MDSC differentiation and function by activation of
673 GCN2. (2023) doi:10.1101/2023.08.09.552588.

674 27. Yan, G. *et al.* Integrated Stress Response Potentiates Ponatinib-Induced Cardiotoxicity.
675 *Circ. Res.* (2024) doi:10.1161/circresaha.123.323683.

676 28. Abramson, J. *et al.* Accurate structure prediction of biomolecular interactions with
677 AlphaFold 3. *Nature* 1–3 (2024) doi:10.1038/s41586-024-07487-w.

678 29. Mirdita, M. *et al.* ColabFold: making protein folding accessible to all. *Nat. Methods* **19**,
679 679–682 (2022).

680 30. Gárriz, A. *et al.* A Network of Hydrophobic Residues Impeding Helix αC Rotation
681 Maintains Latency of Kinase Gcn2, Which Phosphorylates the α Subunit of Translation
682 Initiation Factor 2. *Mol. Cell. Biol.* **29**, 1592–1607 (2009).

683 31. Qiu, H., Garcia-Barrio, M. T. & Hinnebusch, A. G. Dimerization by Translation Initiation
684 Factor 2 Kinase GCN2 Is Mediated by Interactions in the C-Terminal Ribosome-Binding
685 Region and the Protein Kinase Domain. *Molecular and Cellular Biology* **18**, 2697–2711
686 (1998).

687 32. Qiu, H., Dong, J., Hu, C., Francklyn, C. S. & Hinnebusch, A. G. The tRNA-binding moiety
688 in GCN2 contains a dimerization domain that interacts with the kinase domain and is
689 required for tRNA binding and kinase activation. *Embo J* **20**, 1425–1438 (2001).

690 33. Yin, J. Z. *et al.* The HisRS-like domain of GCN2 is a pseudoenzyme that can bind
691 uncharged tRNA. *Structure* (2024) doi:10.1016/j.str.2024.02.021.

692 34. Stonyte, V. *et al.* The GCN2/eIF2αK stress kinase regulates PP1 to ensure mitotic
693 fidelity. *EMBO Rep.* **24**, e56100 (2023).

694 35. Hatzivassiliou, G. *et al.* RAF inhibitors prime wild-type RAF to activate the MAPK
695 pathway and enhance growth. *Nature* **464**, 431–435 (2010).

696 36. Poulikakos, P. I., Zhang, C., Bollag, G., Shokat, K. M. & Rosen, N. RAF inhibitors
697 transactivate RAF dimers and ERK signalling in cells with wild-type BRAF. *Nature* **464**, 427–
698 430 (2010).

699 37. Lageix, S., Zhang, J., Rothenburg, S. & Hinnebusch, A. G. Interaction between the
700 tRNA-binding and C-terminal domains of Yeast Gcn2 regulates kinase activity in vivo. *PLoS*
701 *genetics* **11**, e1004991 (2015).

702 38. Lageix, S., Rothenburg, S., Dever, T. E. & Hinnebusch, A. G. Enhanced Interaction
703 between Pseudokinase and Kinase Domains in Gcn2 stimulates eIF2α Phosphorylation in
704 Starved Cells. *PLoS Genet.* **10**, e1004326 (2015).

705 39. Oliveira, Tm. *et al.* The structure of human GCN2 reveals a parallel, back-to-back kinase
706 dimer with a plastic DFG activation loop motif. *Biochem J* **477**, 275–284 (2020).

707 40. Masson, G. R., Maslen, S. L. & Williams, R. L. Analysis of phosphoinositide 3-kinase
708 inhibitors by bottom-up electron-transfer dissociation hydrogen/deuterium exchange mass
709 spectrometry. *The Biochemical journal* **474**, 1867–1877 (2017).

710 41. Gajiwala, K. S. *et al.* KIT kinase mutants show unique mechanisms of drug resistance to
711 imatinib and sunitinib in gastrointestinal stromal tumor patients. *Proc. Natl. Acad. Sci.* **106**,
712 1542–1547 (2009).

713 42. Trebino, T. E., Markusic, B., Nan, H., Banerjee, S. & Wang, Z. Unveiling the domain-
714 specific and RAS isoform-specific details of BRAF kinase regulation. *eLife* **12**, RP88836
715 (2023).

716 43. Anderson, J. W. *et al.* Conformation selection by ATP-competitive inhibitors and
717 allosteric communication in ERK2. *eLife* **12**, RP91507 (2024).

718 44. Gong, G. Q. *et al.* A small-molecule PI3Kα activator for cardioprotection and
719 neuroregeneration. *Nature* 1–10 (2023) doi:10.1038/s41586-023-05972-2.

720 45. Dey, M., Cao, C., Sicheri, F. & Dever, T. E. Conserved intermolecular salt bridge
721 required for activation of protein kinases PKR, GCN2, and PERK. *Journal of Biological*
722 *Chemistry* **282**, 6653–6660 (2007).

723 46. Padyana, A. K., Qiu, H., Roll-Mecak, A., Hinnebusch, A. G. & Burley, S. K. Structural
724 Basis for Autoinhibition and Mutational Activation of Eukaryotic Initiation Factor 2α Protein
725 Kinase GCN2. *J Biol Chem* **280**, 29289–29299 (2005).

726 47. He, H. *et al.* Crystal structures of GCN2 protein kinase C-terminal domains suggest
727 regulatory differences in yeast and mammals. *The Journal of biological chemistry* **289**,
728 15023–15034 (2014).

729 48. Ramirez, M., Wek, R. C. & Hinnebusch, A. G. Ribosome association of GCN2 protein
730 kinase, a translational activator of the GCN4 gene of Saccharomyces cerevisiae. *Mol. Cell.*
731 *Biol.* **11**, 3027–3036 (1991).

732 49. Gold, L. T. & Masson, G. R. GCN2: roles in tumour development and progression.
733 *Biochem Soc T* **50**, 737–745 (2022).

734 50. Gold, L. T. *et al.* The amino-acid stress sensing eIF2α kinase GCN2 is a survival
735 biomarker for malignant mesothelioma. *BJC Rep.* **1**, 4 (2022).

736

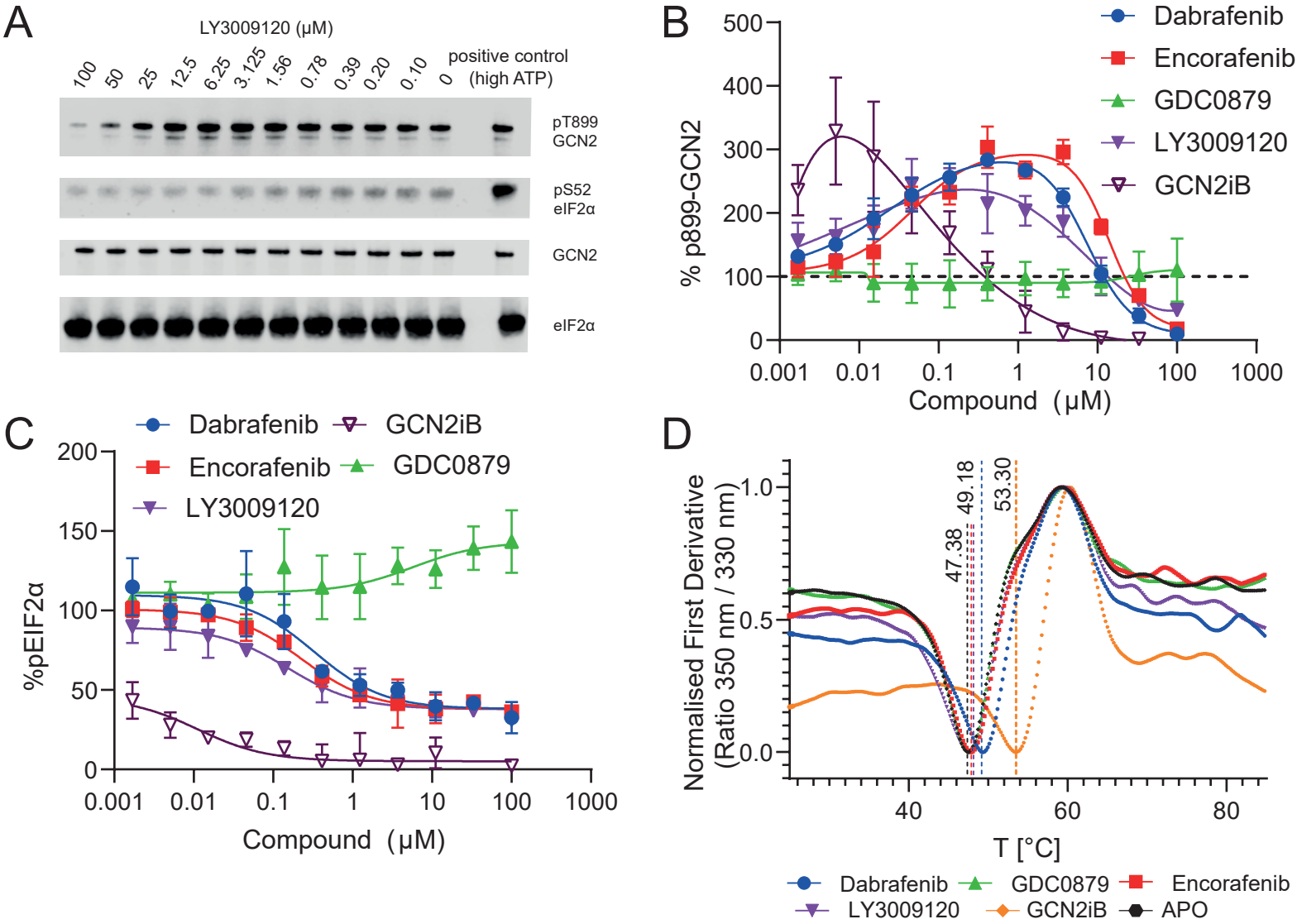


**Figure 1**: RAFi and GCN2iB promote GCN2 autophosphorylation, but not eIF2α phosphorylation. (A) Activity assay of human recombinant GCN2 phosphorylating eIF2α against a concentration gradient of LY3009120. (B) Quantified assays against 5 compounds – LY3009120, Dabrafenib, Encorafenib, GDC0879 and GCN2iB. pThr899 GCN2 levels peak at ~1 μM for Dabrafenib, Encorafenib and GDC0879, and 10 nM for GCN2iB. GDC0879 does not appear to alter GCN2 activity (C) pS51 EIF2α levels across a gradient of compounds. (D) Thermal Unfolding assays of GCN2 against compounds. Lines represent nadirs of the first inflection point.

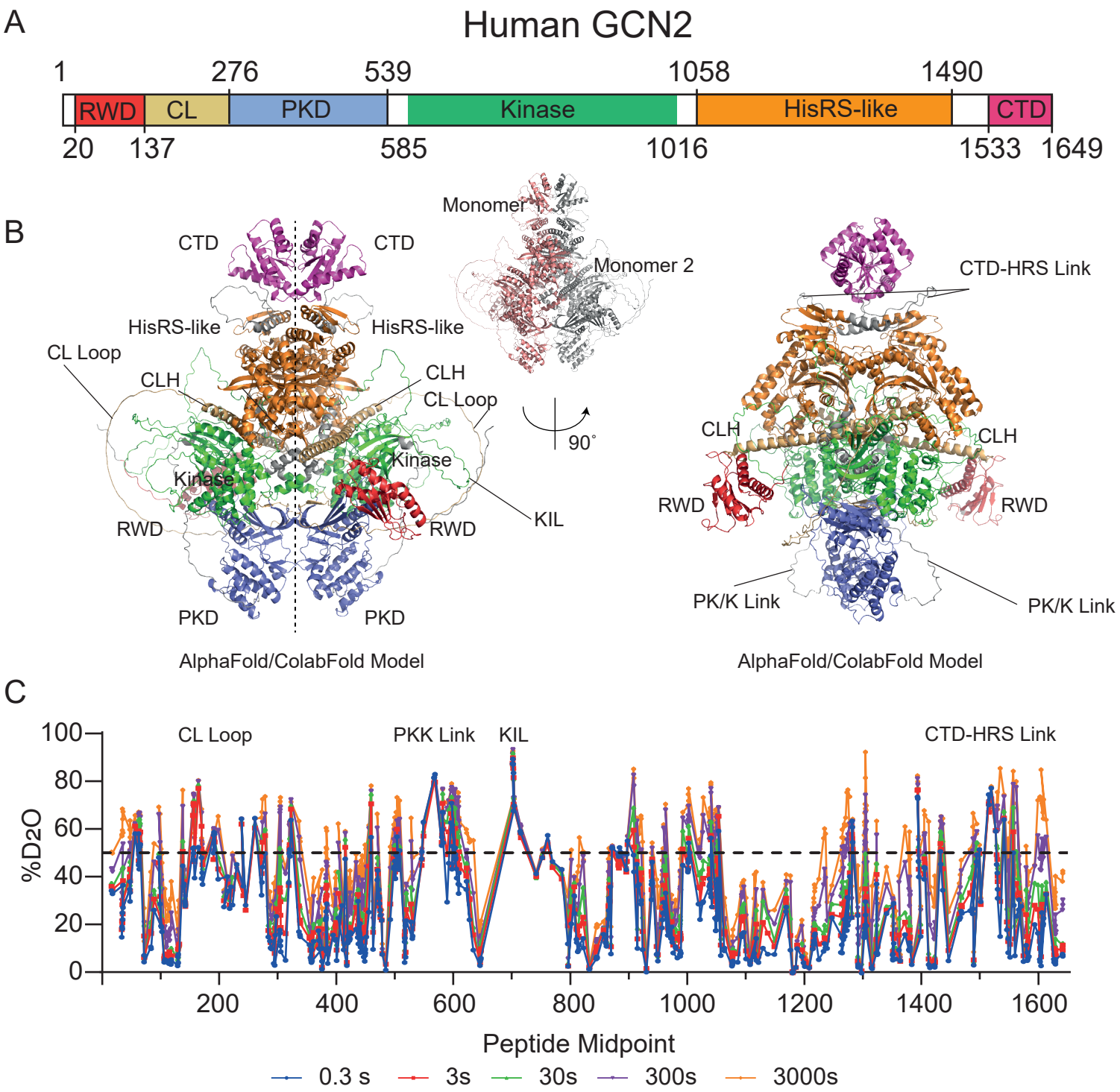


**Figure 2**: Predicted Model of GCN2 generated by AlphaFold/Collabfold and comparison to HDX-MS data. (A) Domain organisation and amino acid residue boundaries for human GCN2. CL = Charged Linker, PKD = pseudokinase domain, HisRS = Histidyl synthetase like domain, CTD = C-terminal Domain (B) Views of the GCN2 dimer generated using AlphaFold/Colabfold. CLH = charged linker helix, KIL = kinase insertion loop. (C) HDX-MS data for APO GCN2. Typically, regions where deuterium uptake is greater than 50% (shown as the dashed line) at 0.3s incorporation are likely unstructured loops with his flexibility.

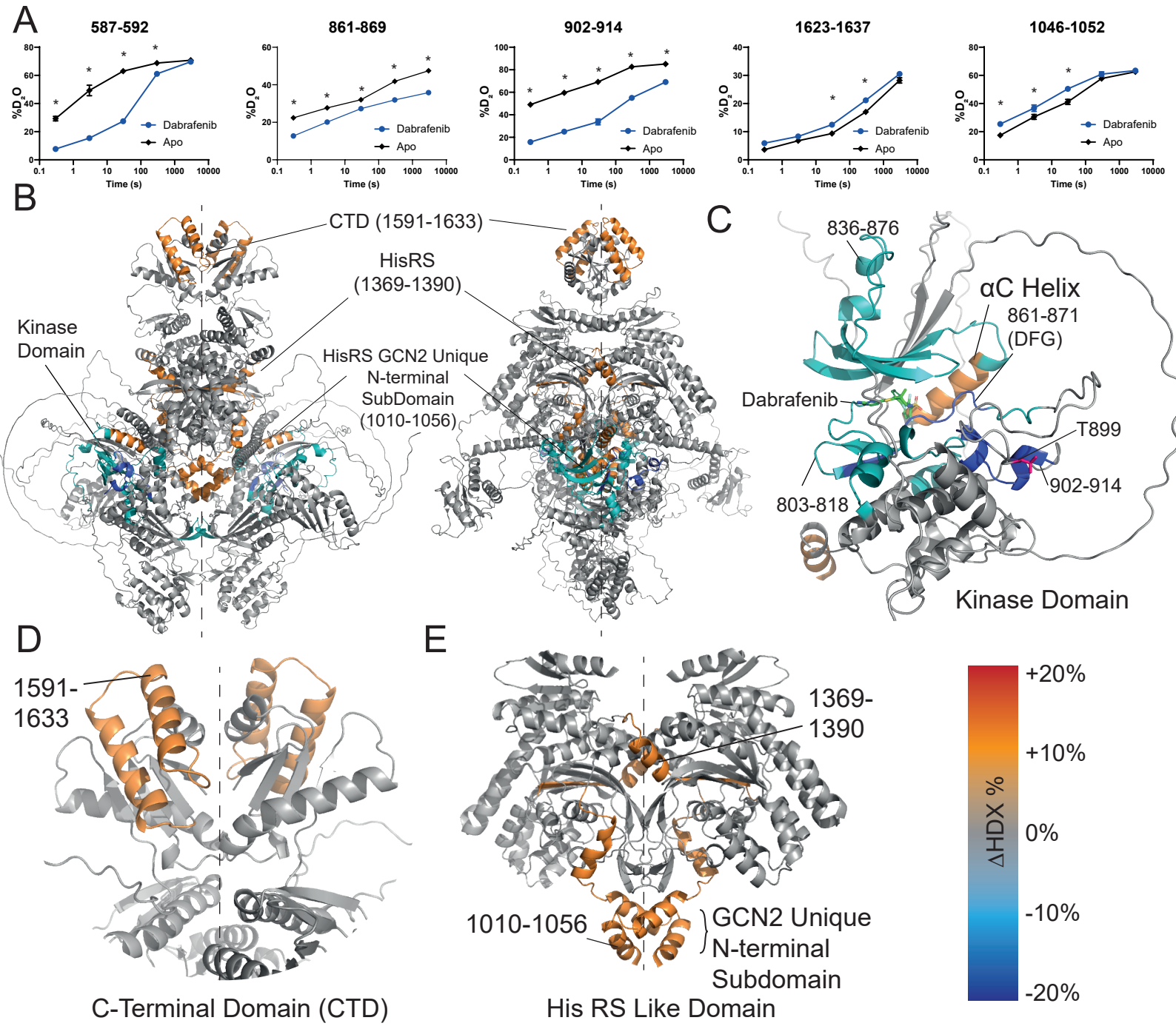


**Figure 3:** HDX-MS changes associated with Dabrafenib binding. (A) Selected peptides showing the effect of Dabrafenib binding to GCN2. * = Greater than 5% & 0.5Da change, passes t-test at p=0.05. Error bars may be smaller than the points on the graph. (B) Dabrafenib binding mapped onto the entire GCN2 model. Cooler colours represent areas of 'protection' (i.e., slower solvent exchange rate), warmer colours show 'exposure' (i.e., increased solvent exchange rate). (C) Inset of the kinase domain of GCN2 showing HDX changes on Dabrafenib binding. T899, a "bell weather" site of autophosphorylation and activation is highlighted. (D) The C-Terminal Domain of GCN2, highlighting the exposure of the helical hairpin found in residues 1591-1633. (E) The His-RS Like Domain with the GCN2 Unique N-terminal Subdomain included, highlight the exposure occurring in this domain. Dashed lines represent 2-fold symmetry of the dimer.

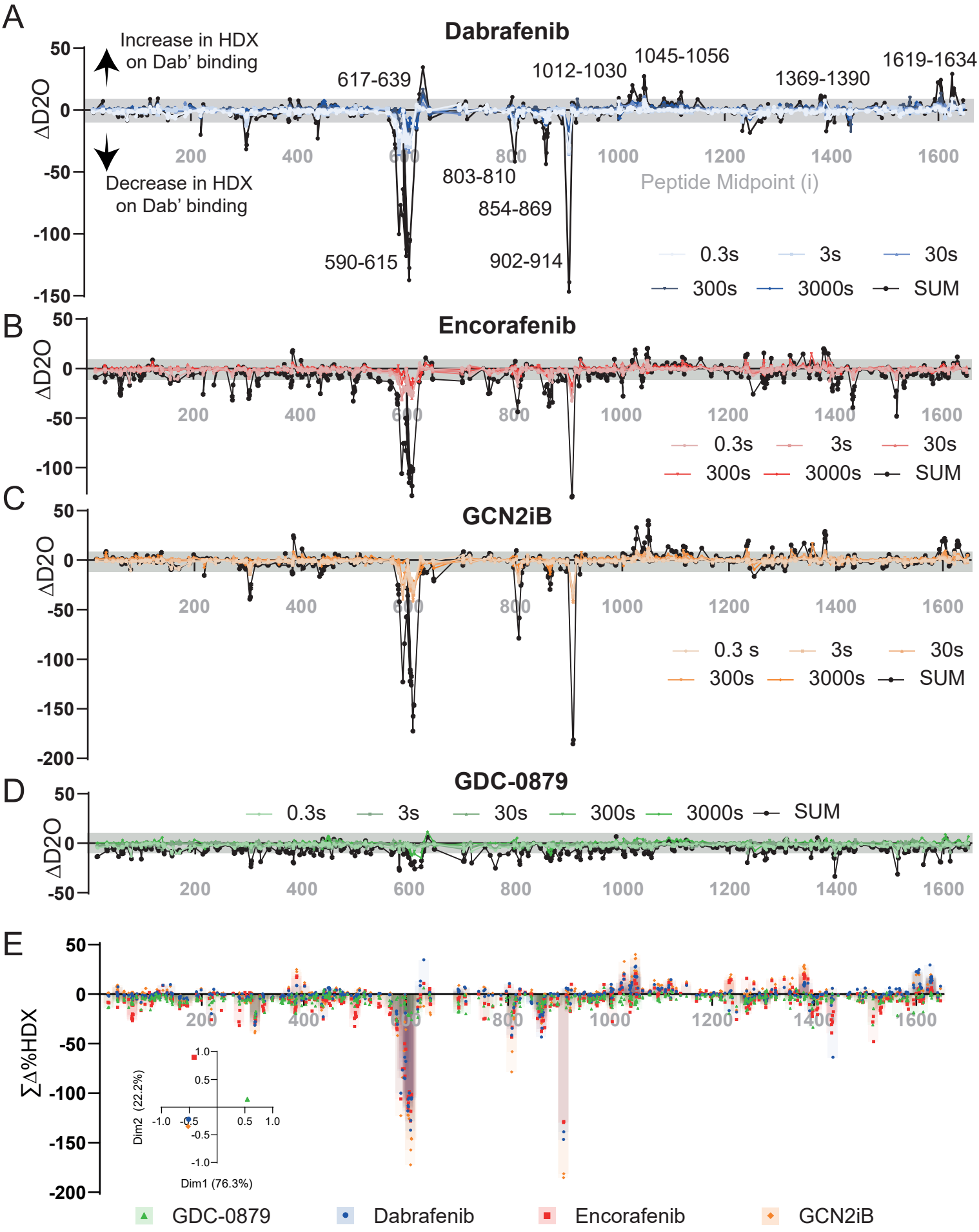


**Figure 4:** Comparison of HDX-MS changes with (A) Dabrafenib (B) Encorafenib (C) GCN2iB (D) GDC0876. Each point in the midpoint of a peptide with the five-points in gradually more saturated colours. Black points/line are the SUM difference across all timepoints. (E) Amalgamated changes mapped onto one another. Inset is a principal component analysis comparing all the data summed data.

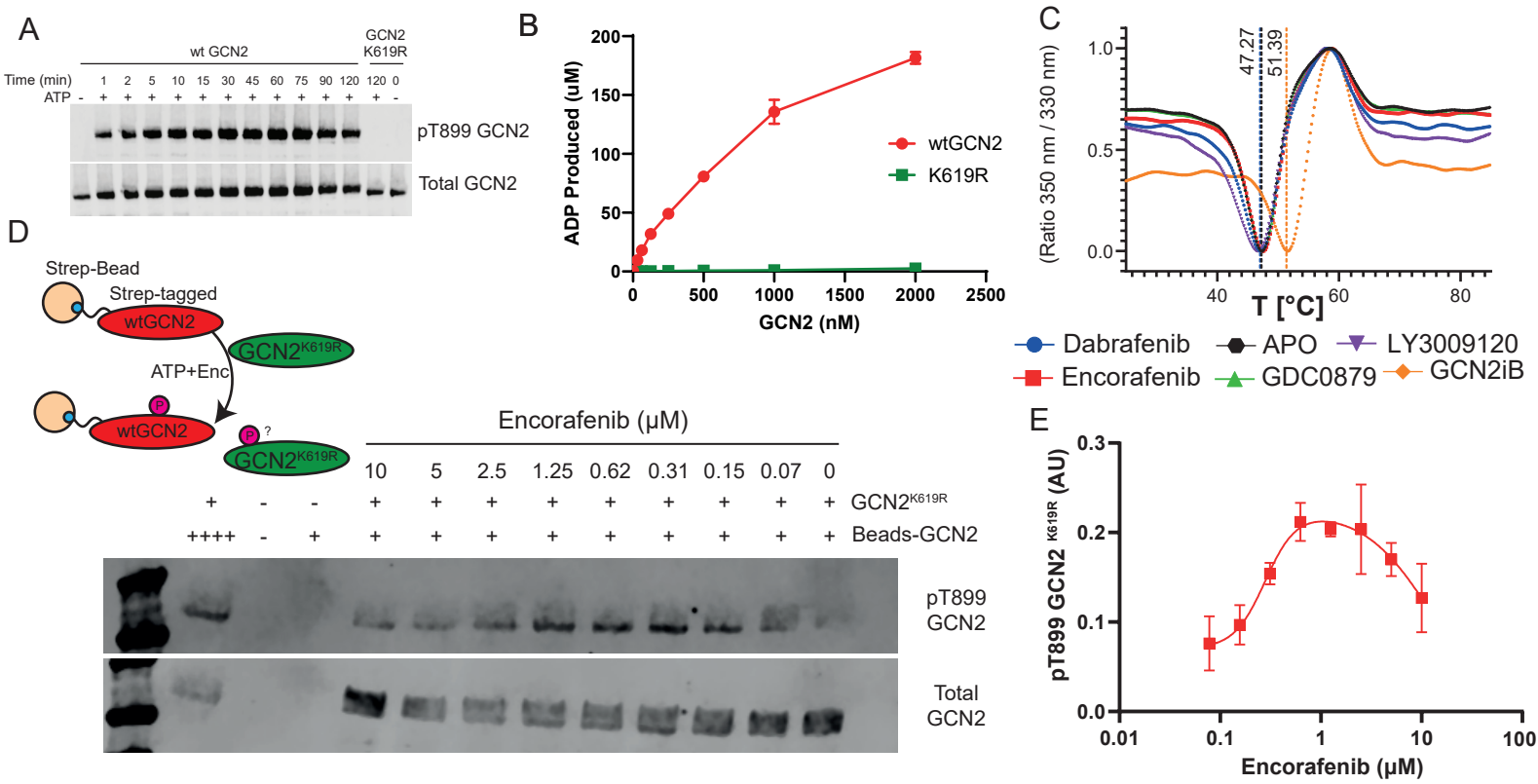


**Figure 5:** GCN2 is capable of phosphorylating in trans (A) Autophosphorylation activity comparison of wtGCN2 with GCN2K619R. (B) Comparison of ATPase activity as measured using ADPGLO between GCN2 and GCN2K619R. (C) Thermal Unfolding Assay for GCN2K619R on compound binding. (D) Western Blot analysis of trans-phosphorylation of GCN2. (E) Compound-driven trans phosphorylation of GCN2K619R by immobilised wtGCN2 by Encorafenib.

A

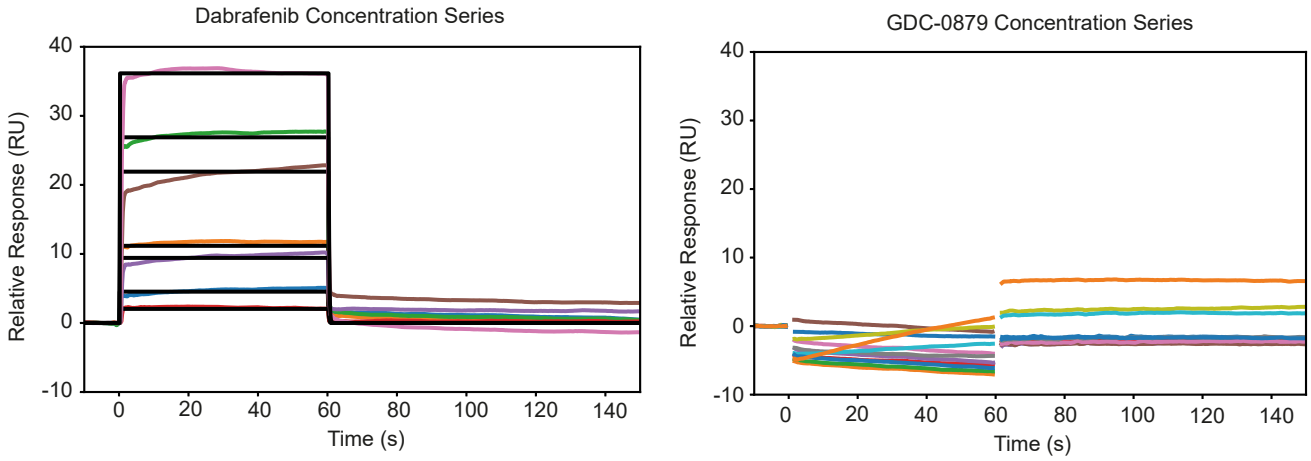


B

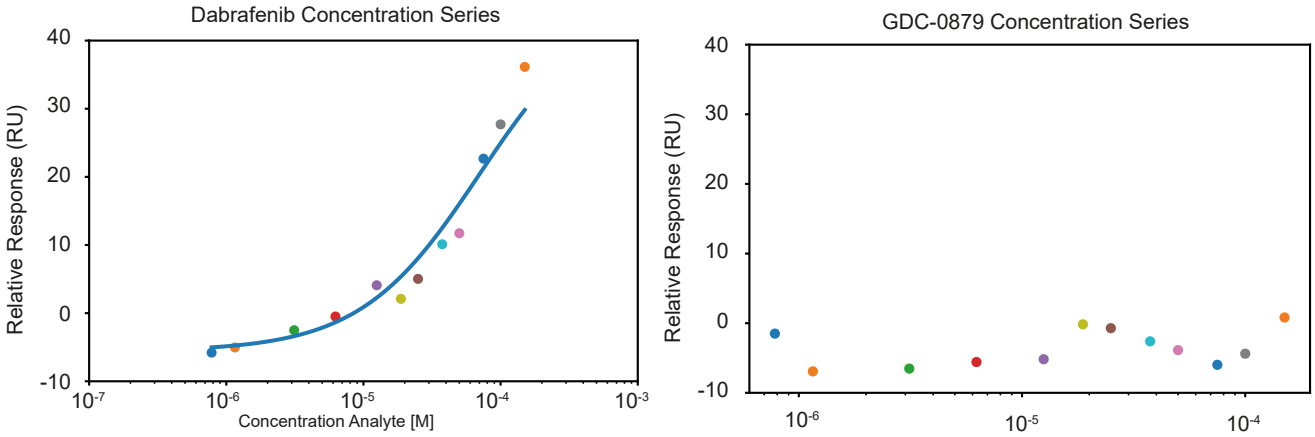


C

| | $K_D^{SPR}$ | $\Delta T_m$ |
|---|---|---|
| Dabrafenib | 70.8 μM ± 8.3 | +2.1 ˚C ± 0.4 |
| Encorafenib | Req> 0.5·Rmax | +0.8 ˚C ± 0.2 |
| LY3009120 | 43.1 μM ± 2.5 | +0.6 ˚C ± 0.3 |
| GCN2iB | Req> 0.5·Rmax | +5.9 ˚C ± 0.1 |
| GDC-0879 | No binding detected | No shift detected |

**Supplementary Figure 1:** Binding of Compounds to GCN2 (A) SPR traces of binder Dabrafenib and non-binder GDC-0879 (B) Steady-State analysis of compound binding derived from SPR (C) Amalgamated compound characteristics. *Analytes including Encorafenib and GCN2iB demonstrated binding with SPR, producing a concentration dependent response, but at the analytes at higher concentrations shows superstoichiometry or binding without complete saturation of the ligand in the concentration range used 51. The affinities, as determined by kinetic analysis, could not be reliably determined.

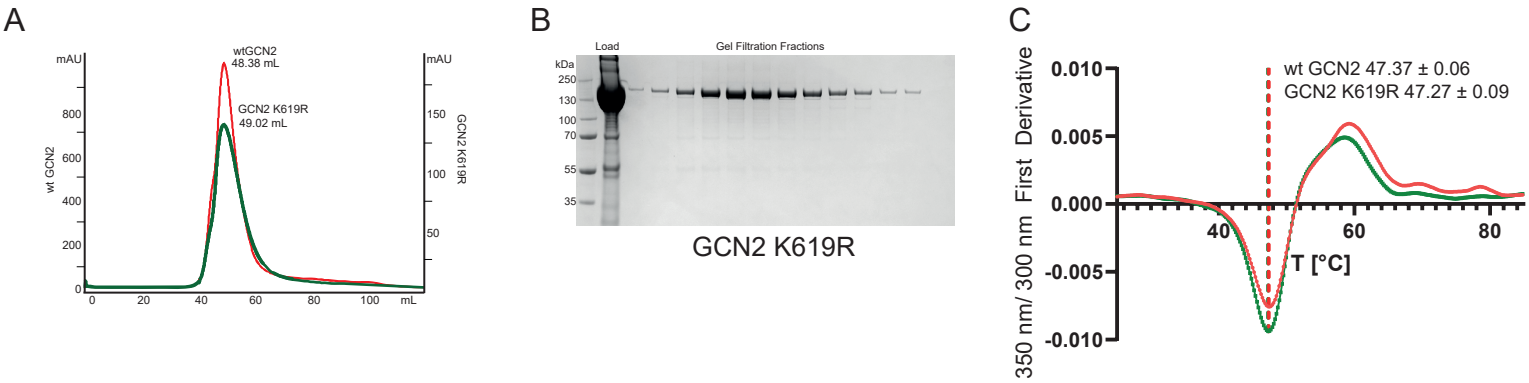


**Supplementary Figure 2:** Characterisation of GCN2K619R (A) Gel Filtration profile of wtGCN2 (red) and GCN2K619R (green) showing similar elution profiles (B) SDS-PAGE of Gel Filtration of fractions of GCN2K619R (C) Thermal denaturation profile of wtGCN2 (red) and GCN2K619R (green).

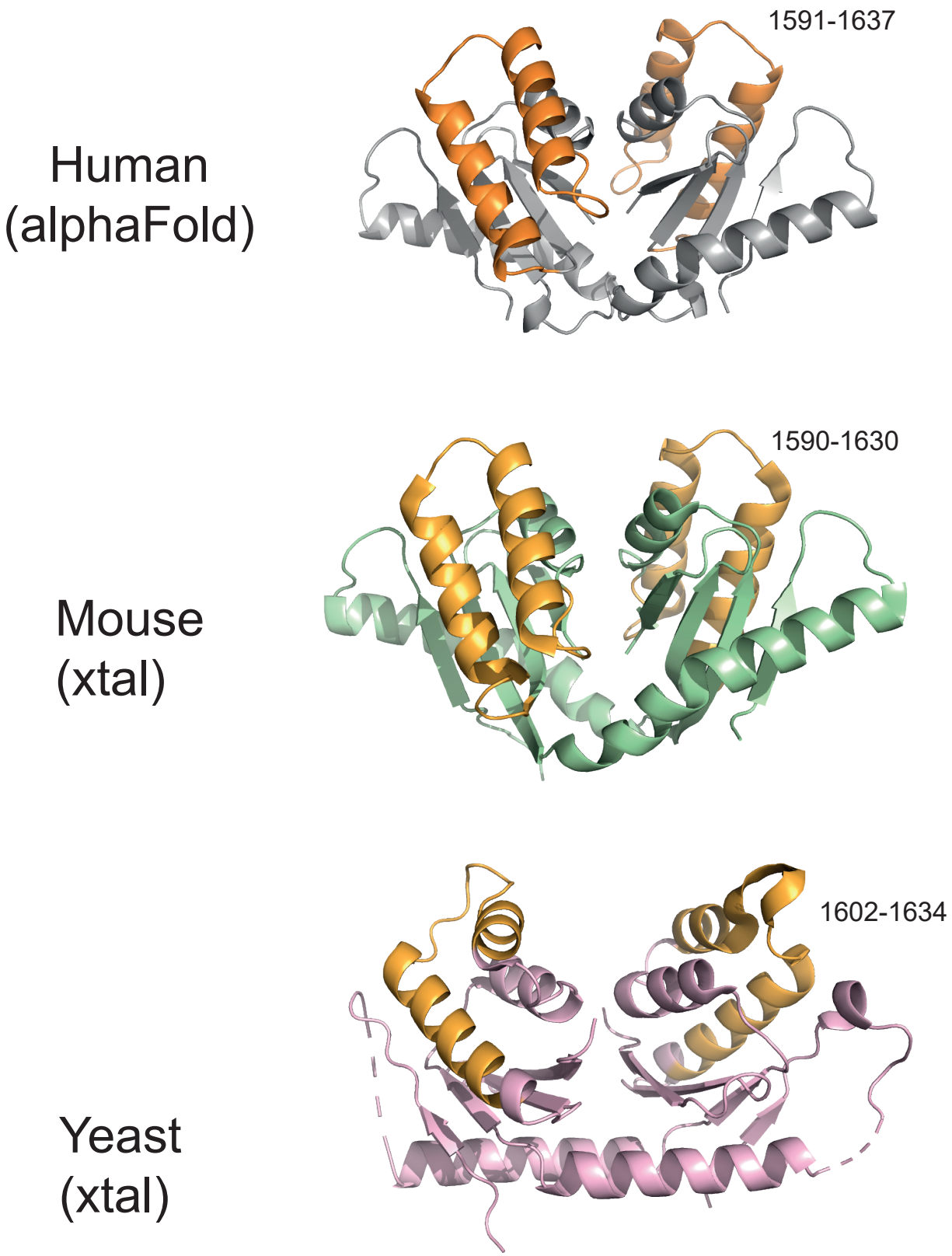


**Supplementary Figure 3:** Comparison of CTDs. The CTDs of Human (produced by Alphafold), Mouse (crystal structure PDB: 4OTN), and Yeast (4OTM), with the helix-turn-helix motif which exhibited an increase in HDX-MS on compound binding shown in orange.